EFFECT OF CRYOGENIC TREATMENT AND THERMAL SHOCK ON RESIDUAL STRESSES, STRUCTURE AND PROPERTIES OF ALLOY D16

Yu. A. Puchkov,[1] Mai Xuan Dung,[1] A. I. Plokhikh,[1] I. Benarieb,[2] R. M. Nazarkin,[2] and W. A. Pancho Ramires[1]

The effect of heat treatment involving water quenching, cooling of the quenched alloy in liquid nitrogen, a hold in liquid nitrogen, heating in hot mineral oil (thermal shock), and natural or artificial aging on the structure and properties of deformable aluminum alloy D16 is studied. The structure of the alloy is analyzed by optical and transmission electron microscopy and x-ray diffraction analysis. The effect of the heat treatments on the residual microstresses is determined by the method of drilling holes, and the mechanical properties of D16 are determined in tensile tests.

Key words: heat treatment, cryogenic treatment, thermal shock, aluminum alloys, microstructure, D16, residual stresses, mechanical properties.

INTRODUCTION

Quenching and aging raise considerably the structural strength of aluminum alloys but cause undesirable macrostresses. Macrostresses result in elastic and plastic deformation, warpage, higher allowances and volume of mechanical processing, worsening of the processing accuracy and size stability of the articles and may lower their strength, reliability and endurance [1]. In some cases, aging does not reduce the residual macrostresses to the required level, because it is accompanied by formation of fine hardening particles hindering the motion of dislocations and stress relaxation. Warpage and residual macrostresses are lowered by choosing quenching cooling media and their temperatures. It is expedient to choose the quenchant using the quenching factor method, which is implemented after determination of the mode of cooling at various points of the article (for example, with the help of the ANSYS software), of the temperature-time-property diagram (the diagram of attainment of properties) of the treated alloy, and with the help of a special software [2 – 6].

The process of hardening of aluminum alloys can be advanced using a still insufficiently popular technology involving cryogenic treatment and thermal shock (CTTS) [7 – 10]. In this case, the articles are water cooled to a low temperature, for example, by immersing into liquid nitrogen, and then heated rapidly in boiling water, high-speed steam, or hot oil. This treatment is accompanied by plastic deformation under cryogenic temperature during the thermal shock. The changes in the structure of the alloys under CTTS have not been studied exhaustively. However, the influence of plastic deformation on the structure and properties of aluminum alloys at cryogenic temperatures has been investigated. Tensile tests of alloys EN 1085, EN 5182 and ENAW 6016 have shown [11] that decrease in the temperature from 25 to –196°C elevates their yield strength, ultimate tensile strength and elongation. The elevation of the properties is largely a result of growth of the rate of strain hardening at cryogenic temperatures and may be associated with shortening of the stage of dynamic retrogression due to transverse slip of helical dislocations. This agrees well with the growth in the dislocation density and elevation of the fraction of helical dislocations at low deformation temperatures.

The use of CTTS instead of the conventional heat treatment lowers considerably the level of residual stresses in the articles [12 – 14]. The residual stresses and the warpage become lower under the thermal shock because the direction of

[1] Bauman Moscow State Technical University (BMSTU), Moscow, Russia (e-mail: Putchkov bmstu@mail.ru).

[2] Research Center "Kurchatov Institute" – FSUE "All-Russia Scientific Research Institute of Aviation Materials" (VIAM), Moscow, Russia.

TABLE 1. Modes of Heat Treatment of Specimens of Alloy D16

Mode	Heat treatment stage			
	Quenching	Cryogenic treatment	Thermal shock	Aging
1 (CTTS)	Heating in a salt bath to 495 ± 2°C, holding for 20 min, water cooling at 40 ± 1°C for 5 min	Cooling to –196°C, holding in liquid nitrogen for 5 min (ring specimens) and for 15 min (rectangular specimens)	Heating from –196°C to 175 ± 2°C (in oil) for 5 min	190 ± 1°C, 12 h
2 (CTTS)				20 ± 2°C, 100 h
3	Not conducted		Not conducted	190 ± 1°C, 12 h
4	Not conducted		Not conducted	20 ± 2°C, 100 h

the stresses and of the strain is opposite to that of the stresses and of the strain arising under the preliminary quenching. The thermal shock causes plastic deformation in the surface zone of the alloy, i.e., is a kind of surface hardening raising the structural strength of the article.

The method of CTTS can be applied to precision shaped large-size and thick-wall articles such as tubes [15], ailerons, longerons, fuselage parts, frames of inertial positioning systems, landing gear housings, liners, cylinder blocks, bosses, large mirrors of optical telescopes, etc. [1].

The aim of the present work was to study the effect of cryogenic treatment and thermal shock followed by natural or artificial aging on the structure, residual stresses and mechanical properties of alloy D16.

METHODS OF STUDY

We studied aluminum alloy D16. Ring specimens with external diameter 60 mm, internal diameter 40 mm and width 10 mm were cut from pressed bars to conduct the study. Rectangular specimens with a size of 100 × 30 × 25 mm and cylindrical specimens of type VII (GOST 1497–84) with functional part 6 mm in diameter were cut from a plate with a thickness of 25 mm. A "LAES" atomic emission spectrometer with laser excitation was used to determine the chemical composition of the alloy (in wt.%), i.e., 4.35 Cu, 1.50 Mg, 0.60 Mn, 0.50 Si, 0.50 Fe, 0.10 Zn, 0.16 Cr, 0.07 Ti, the remainder Al.

The alloy was heat treated in shaft furnaces. The succession and the modes of the heat treatment are presented in Table 1. The temperature in the salt and oil tanks was kept with the help of certified chromel-alumel thermocouples and a 2TRM1-Shch2.U.RR microprocessor temperature controller. The working medium in the salt tank was a mixture of 55% $NaNO_3$ + 45% $NaNO_2$; that in the oil tank was Termoil 26. To level the temperature in the tanks, the solution was stirred thoroughly during cooling of the specimens. The specimens after treatments *1* and *3* were subjected to artificial aging in a BINDER ED-23 chamber furnace for 12 h; those after treatments *2* and *4* were aged naturally for 100 h.

The changes in the structure were studied using an Olympus GX51 optical microscope, a JEM-2000 EX electron transmission microscope and a DRON-4 diffractometer.

The residual stresses in the specimens were determined by the drilling method according to ASTM E837-08 using type B strain gages. The specimens were drilled perpendicularly to the outer cylindrical surface to a depth of 2 mm with a conical end milling cutter 1.8 mm in diameter. The residual stresses were determined using a bridge circuit.

The maximum (σ_{max}) and minimum (σ_{min}) residual stresses were calculated by the equation

$$\sigma_{max}, \sigma_{min} = \frac{E}{2(1-\nu^2)} \times [(1+\nu)(\varepsilon_a + \varepsilon_c) \pm$$
$$(1-\nu) \times \sqrt{2\{(\varepsilon_a - \varepsilon_b)^2 + (\varepsilon_b - \varepsilon_c)^2\}}],$$

where ε_a, ε_b, ε_c are the measured strains in directions *a*, *b*, *c*, respectively, going at an angle of 45°; ν is the Poisson coefficient; and *E* is the modulus of elasticity.

The microhardness of the specimens was measured using an EMCO-TEST Durascan 20 hardness tester by the Vickers method at a load of 100 g with a hold for 10 sec in accordance with GOST R ISO 6507-1–2007.

The electrical conductivity of the surface zones of the specimens was determined using a VE-27NTs eddy-current meter for analyzing the parameters (the phase) of the electromagnetic field of the eddy currents under the interaction between the eddy-current sensor of the device and the surface layer of the metal studied.

The tests for static tension were conducted according to GOST 1497–84 in a Z100 "Zwick/Roell" tension testing machine. The main characteristics were calculated automatically using a standard software for data acquisition and processing.

RESULTS AND DISCUSSION

Figure 1 presents the diffraction patterns of alloy D16 after two kinds of heat treatment, i.e., (*1*) quenching, CTTS and artificial aging and (*2*) quenching and artificial aging. The peaks corresponding to the reflections from planes (111), (200), (220) and 311) of the aluminum-base solid solution have the highest intensity. CTTS does not cause appearance of new peaks from the specimens, which means that no new phase has appeared. However, CTTS changes the pro-
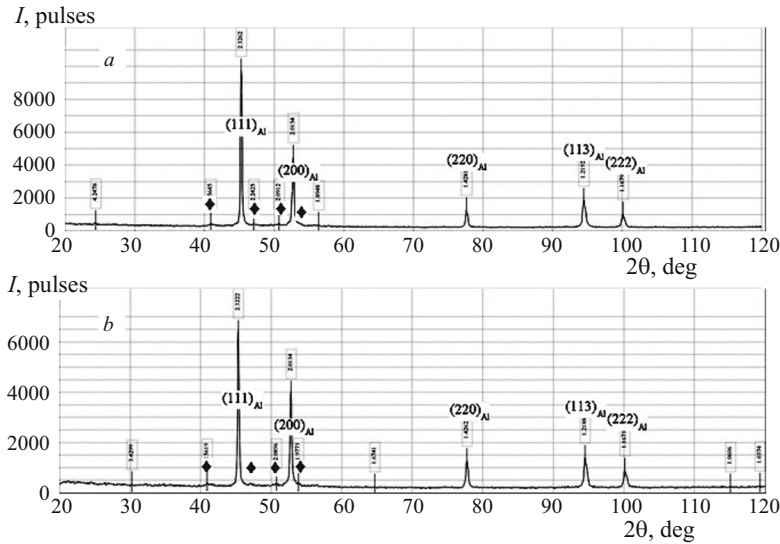
Fig. 1. Diffraction patterns of deformable aluminum alloy D16 after different heat treatments: *a*) quenching, CTTS, and artificial aging; *b*) quenching and artificial aging; ◆) position of reflection from *S*-phase.

TABLE 2. Relative Intensity of Diffraction Peaks $I_{(hkl)}/I_{(111)}$ after Different Treatments

Treatment	$I_{(111)}/I_{(111)}$, %	$I_{(200)}/I_{(111)}$, %	$I_{(220)}/I_{(111)}$, %	$I_{(311)}/I_{(111)}$, %	$I_{(222)}/I_{(111)}$, %
Quenching + CTTS + artificial aging	100	45.9	14.3	19.4	10.2
Quenching + artificial aging	100	61.5	20.0	23.1	13.8

portion of the intensities of the peaks. Analyzing the diffraction patterns, we assumed that the intensity of the diffraction peak from plane (111) was equal to 100%. It turned out (Table 2) that the use of CTTS lowered the intensities of peaks (200), (200), (311) and (222). The changes in the intensities of the diffraction peaks show that CTTS raises the fraction of grains with orientation (111). The texture appears due to the deformation caused by the thermal shock.

We determined the mean block size, the microstrain and the microstress using the reflections from crystallographic planes (*HKL*) (111) and (222) by the Scherrer method. We assumed that the blocks had a spherical shape. The diffraction patterns obtained in cobalt K_α radiation were used to compute the mean diameter *D* (nm) of the spherical blocks and the mean squared microstrain ε (%) in the direction over the normal to plane (111) with the help of the PROFILE software. Knowing the microstrain, we used the generalized

TABLE 3. Characteristics of the Fine Structure of the Surface Zone of Rectangular Specimens

Heat treatment	*D*, nm	ε, %	σ, MPa
Quenching + CTTS + artificial aging	70 ± 4	0.11 ± 0.01	56 ± 10
Quenching + artificial aging	88 ± 11	0.14 ± 0.02	100 ± 12

Notations: *D*) average block diameter; ε) mean squared microstrain; σ) microstress.

Hooke's law for the case of uniaxial tension/compression to determine the microstresses σ (MPa). CTTS reduced the mean block diameter and the microstresses (Table 3). The decrease in the size of the blocks is explainable by growth in the dislocation density as a result of the plastic strain due to the thermal shock and formation of new low-angle boundaries. Figure 2 presents the block structure of alloy D16 after different treatments, which was obtained with the help of transmission electron microscopy (TEM). Lath particles of an *S′*-phase are observable on block boundaries.

Optical microscopy (OM) allowed us to detect slip bands in the surface zone of the heat treated rectangular specimens. In the specimens subjected to CTTS, the slip bands were less manifested than after the conventional heat treatment consisting of quenching and artificial aging (Fig. 3*a* and *b*). The cause of the differences is the formation of dislocations as a result of the plastic deformation occurring at the start of the thermal shock when the difference in the temperatures of the specimen and of the hot oil is high and the heat transfer is maximum, because it is controlled by the stage of bubble boiling. As additional cause of formation of dislocations as a result of quenching and cryogenic treatment is supersaturation of the solid solution with vacancies; discs form from vacancies over the closest-packed planes {111}. Collapse of these discs gives rise to subtraction stacking faults. The boundary of these faults can transform into a gliding prismatic dislocation. The formation of faults under the CCTS disrupts partially the quenching-induced slip bands. The CCTS not only raises the dislocation density in the alloy, but
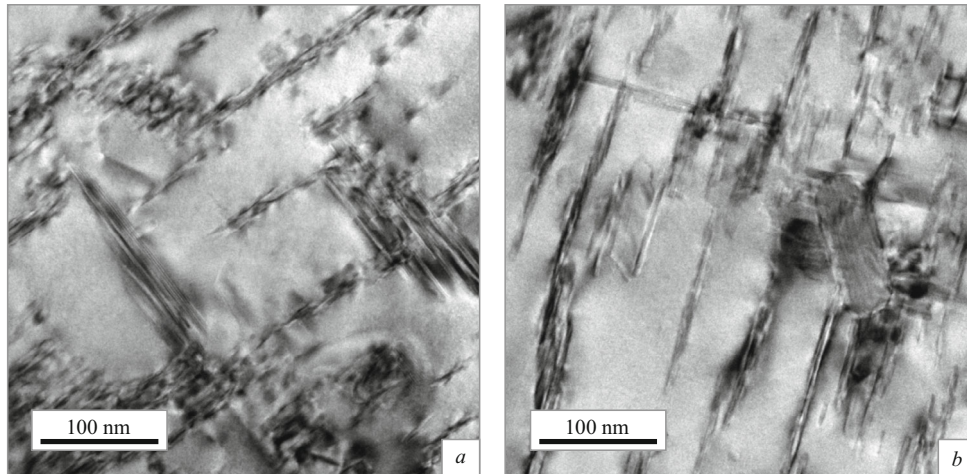
Fig. 2. Block structure of alloy D16 after different treatments: *a*) quenching, CTTS, and artificial aging; *b*) quenching and artificial aging.
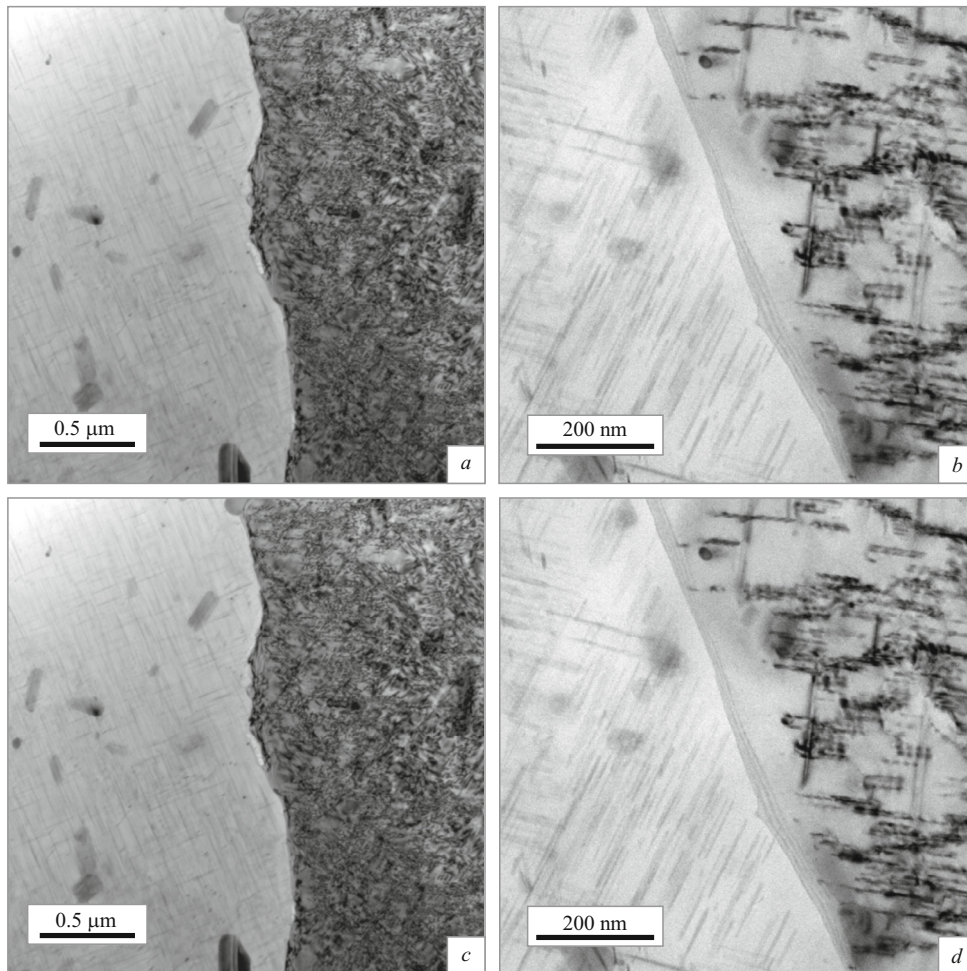

Fig. 3. Microstructure of alloy D16 after different treatments: *a*, *c*) quenching, CTTS, and artificial aging; *b*, *d*) quenching and artificial aging; *a*, *b*) slip bands in the surface zone of specimens; *c*, *d*) absence and presence of a zone free of particles, respectively.

also provides their more uniform distribution. The uniformity of the distribution increases as a result of deceleration of the retrogression and the accompanying lowering of the dislocation mobility as well as the possibility of formation of
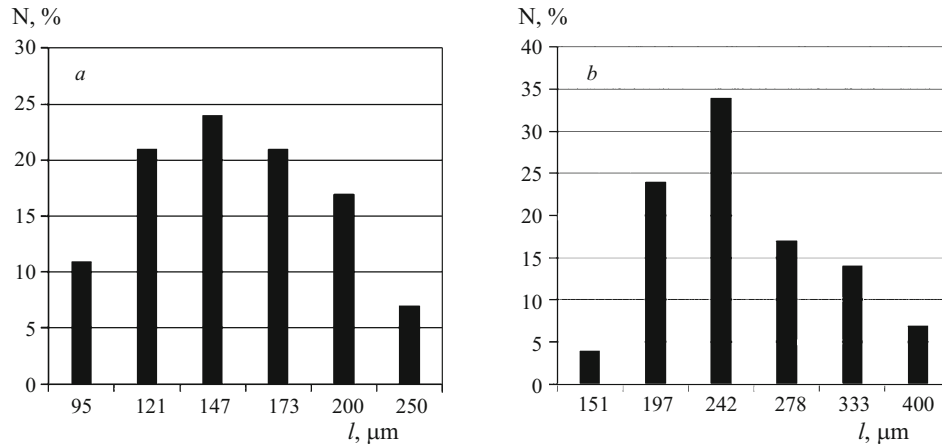
Fig. 4. Size distribution of particles of phase *S'* (*l* is the particle length) in alloy D16 after different treatments: *a*) quenching, CTTS, and artificial aging; *b*) quenching and artificial aging.

dislocation walls. It has been shown in [11] that at –196°C the activation energy of the transverse slip of helical dislocations increases because it depends of the energy of formation of stacking faults, which tends to be reduced in fcc metals at a low temperature. Therefore, the transverse dislocation slip is hindered and the fraction of the helical dislocations increases. After the CTTS, a zone containing no hardening particles, which lowers the strength, does not emerge (Fig. 3*c* and *d*).

Under the aging, the dislocations formed in the CTTS become places of nucleation of finer semi-coherent particles of a hardening *S'*-phase having a lath shape; the size (length) distribution of these laths has an equiaxed nature (Fig. 4). Decrease in the length of these particles seems to be the reason behind the lowering of the microstresses (Table 3).

Figure 5 presents the results of the measurement of the electrical conductivity of the alloy under the outer cylindrical surface of the ring specimens. It can be seen that CTTS raises the conductivity of the alloy. In all probability, this treatment
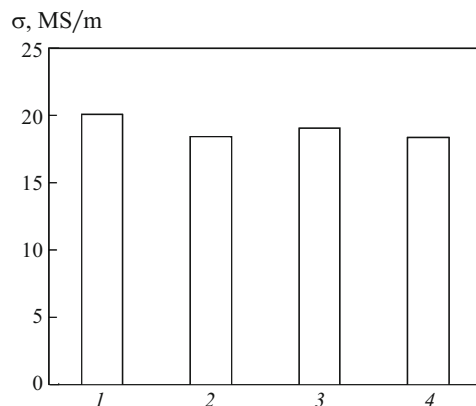
lowers the stresses, which is accompanied by plastic deformation of the surface layer of the metal. As a result, there form dislocations that become centers of nucleation of hardening particles under aging, and this lowers the distortion of the crystal lattice of the matrix solid solution, because its decomposition is more developed.

The study of the fine structure by high-resolution transmission electron microscopy has shown differences in the morphologies of the particles of the hardening phase in alloy D16 after the treatments studied. The CTTS increases the fraction of the semi-coherent lath particles of the *S'*-phase and decreases the content of the massive *S*-phase particles with chiefly incoherent boundaries (Fig. 6).

It is known that small coherent and semi-coherent particles can be cut by dislocations. Artificial aging gives rise to copper- and magnesium-enriched clusters over edge dislocations and then to lath particles of an *S'*-phase. Formation of clusters in a solid solution containing no dislocation is hindered, and this raises the probability of occurrence of massive particles of an *S*-phase with chiefly incoherent boundaries in aluminum alloys [16]. Dislocations can bypass such particles only by bending around, which is accompanied by division of dislocations, mechanical hardening and lowering of the ductility. Dislocations can also bypass the particles of the second phase by the mechanism of local transverse slip, in which they leave behind a prismatic loop, and a dislocation continuing its slip acquires a double step. The loops around the fine particles create fields of elastic stresses that hinder the passage of new dislocations between the particles.

The lath particles grow along habit planes {210] over directions ⟨100⟩$_{Al}$ with orientation relationships $[010]_{(S')}//[021]_{Al}$, $[001]_{(S')}//[012]_{Al}$. The orientation relationship of the faceted particles of the *S*-phase and of the matrix phase is $[021]_S//[041]_{Al}$. These planes are rotated by 22° instead of 26°42′ as in the case of the orientation relationship $[010]_{(S')}//[021]_{Al}$, $[001]_{(S')}//[012]_{Al}$.

Fig. 5. Electrical conductivity of the surface zone under the outer cylindrical surface of ring specimens after treatments *1* and *2* (CTTS) and *3* and *4* (without CTTS).
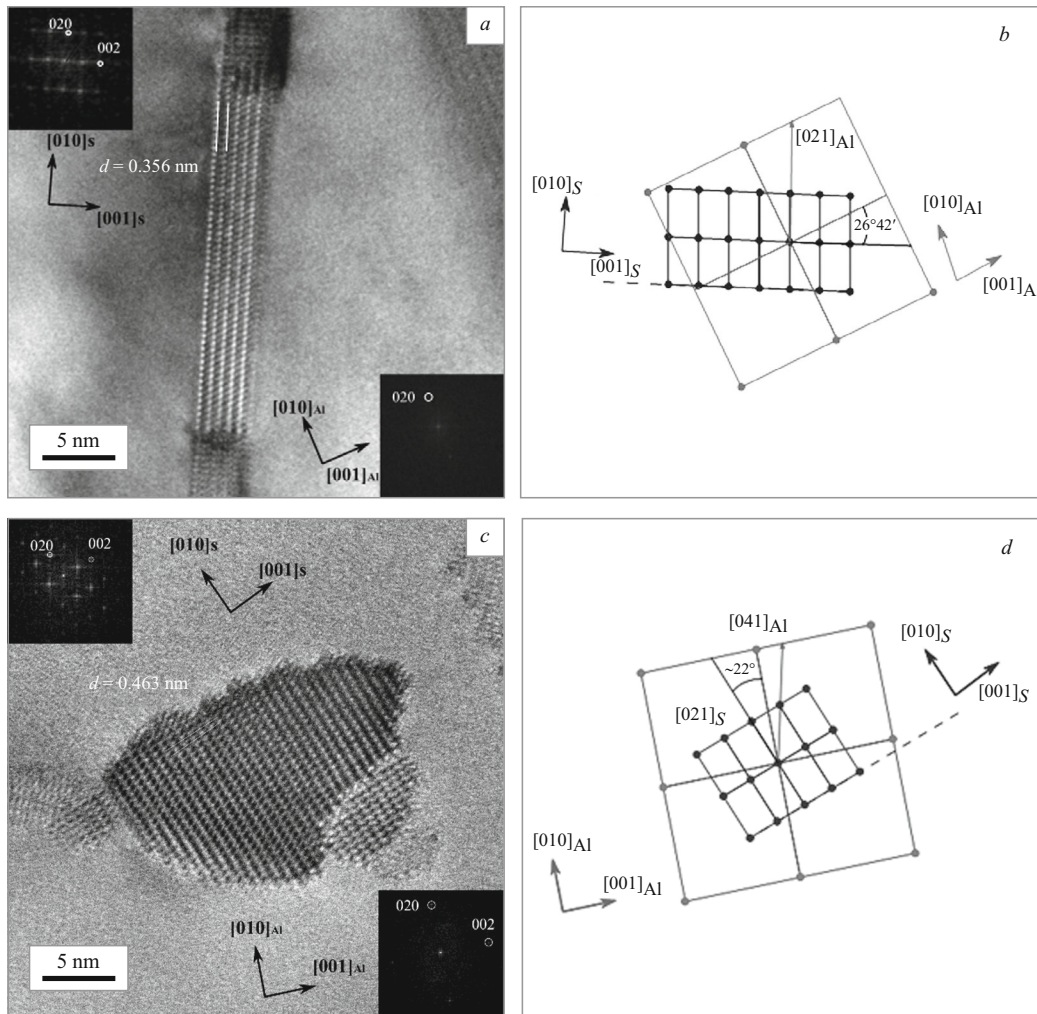
Fig. 6. Lath particles of S'-phase in alloy D16 after CTTS (*a*), faceted particles after the conventional treatment (without CTTS) (*c*), and the respective diagrams of mutual orientation of the crystal lattices of the hardening phase and of the matrix solid solution (*b*, *d*).

The study of the fracture surfaces formed in the tensile tests of alloy D16 gave us data on the effect of the microstructure on the strength and on the ductility. By the data of the microanalysis, the fractures observed after quenching, CTTS and artificial aging and after quenching and artificial aging (Fig. 7) develop by a ductile mechanism (have a lusterless and dimple structure). All the fractures have a relatively flat central part and shear lips in the peripheral part. Near the fracture surface, we observe a contraction typical for ductile fracture.

By the data of the microscopic analysis, the fracture surfaces are mostly represented by regions of ductile fracture and smaller regions of brittle fracture of intermetallic particles. Micropores appear primarily due to the brittle fracture of the particles *T*- and *S*-phases, which causes concentration of plastic flow. The particles of these phases are stress concentrators and places of crack nucleation. The dominant fracture mechanism is formation, growth and coalescence of pores. CTTS raises the ductility of the alloy in tensile tests

(Table 4). It can be assumed that the CTTS reduces the size and raises the uniformity of the distribution of the hardening particles. The zone free of these particles disappears from grain boundaries, the size the detachment dimples decreases, and the ridges on the fracture surface are stretched (Fig. 7*a*).

Figure 8 presents the results of the measurement of microhardness on the side surface of a ring specimen. It can be seen that the microhardness varies by a parabolic law. The hardness is the highest near the outer and inner cylindrical surfaces and the lowest in between. The CTTS raises the hardness by $6 \pm 0.5 \ HV$ after natural aging ad by $4 \pm 0.5 \ HV$ after artificial aging. It seems that this effect may be associated with the plastic deformation and growth in the dislocation density in the thermal shock, because the dislocations serve centers of nucleation of fine hardening particles in subsequent aging.

The properties of the specimens after the CTTS meet the specifications for alloy D16 [17, 18] (Table 4). After the arti-
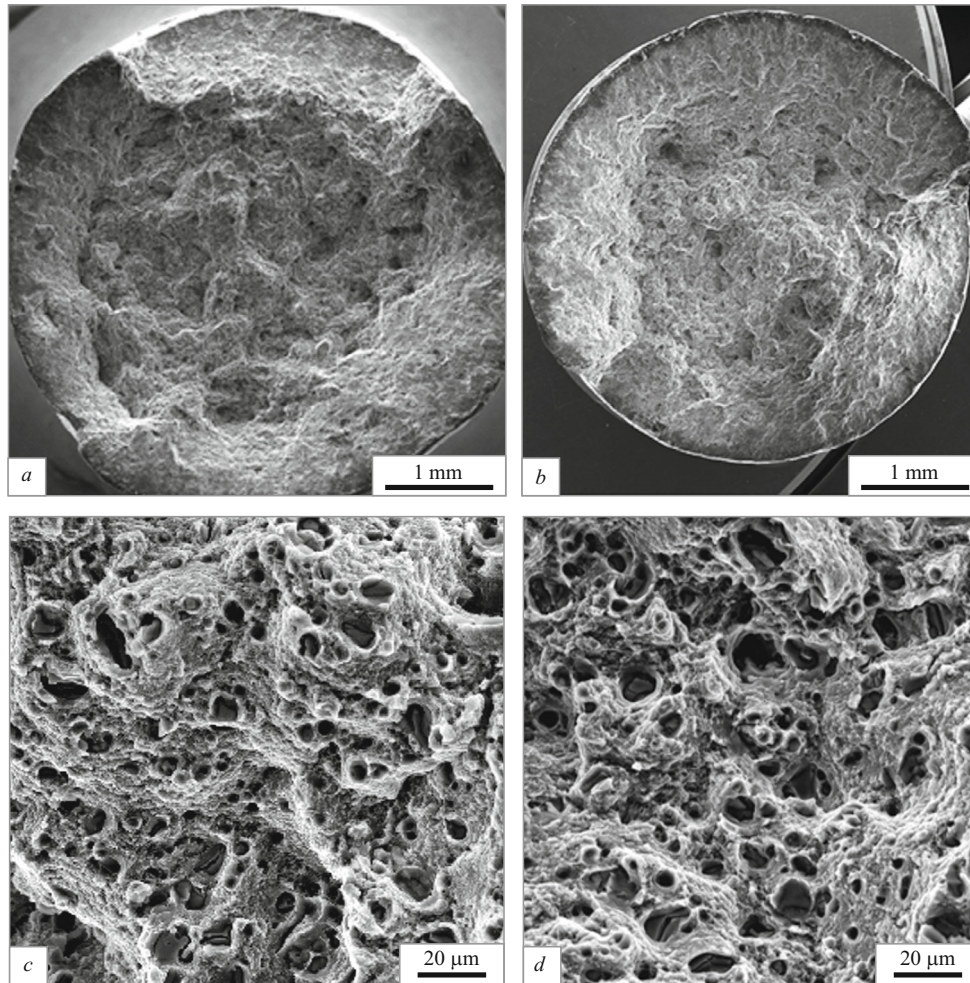
Fig. 7. Fracture surfaces after tensile tests of specimens of alloy D16: *a, c*) quenching, CTTS, and artificial aging; *b, d*) quenching and artificial aging; *a, b*) × 50; *c, d*) × 2000.

ficial aging, their strength is not inferior to that of the specimens subjected to conventional quenching and aging, while their ductility is even superior.

In the case of natural aging, the strength of the alloy subjected to CTTS decreases somewhat, but still exceeds the standardized values (Table 4). The use of CTTS before natural aging may cause some decrease in the strength, which may be associated with lowering of the level of compressive stresses and coarsening of the structure in the surface zone of the specimens in oil heating at a temperature of 175°C before the natural aging.

Figure 9 presents the results of the estimation of residual stresses in ring and rectangular specimens by the method of drilling holes. The use of CTTS lowers the residual stresses in the ring specimens after natural aging from –175 to –130 MPa, i.e., by 26%; after artificial aging, the residual stresses are reduced from –140 to –40 MPa, i.e., by 71%. In rectangular specimens with a size of 100 × 30 × 25 mm, the

TABLE 4. Mechanical Properties of Alloy D16 in Tensile Tests

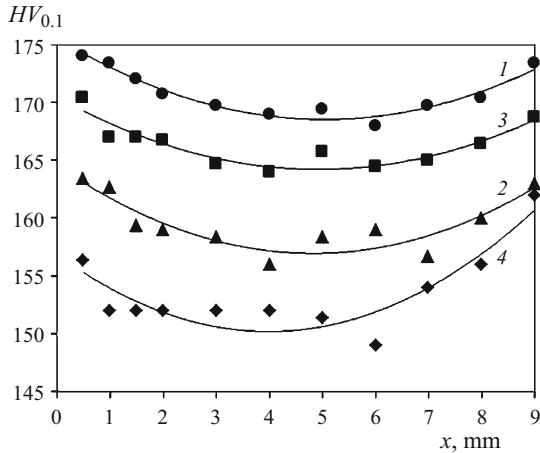| Heat treatment	σ_r, MPa	$\sigma_{0.2}$, MPa	δ, %	ψ, %
Quenching + cryogenic treatment + thermal shock + aging	$\dfrac{460}{470}$	$\dfrac{380}{290}$	$\dfrac{16}{22}$	$\dfrac{26}{30}$
Quenching + aging	$\dfrac{460}{490}$	$\dfrac{380}{330}$	$\dfrac{13}{21}$	$\dfrac{25}{26}$
Standardized values	≥ 425 [17] ≥ 390 [18]	≥ 345 [17] ≥ 275 [18]	≥ 5 [17] ≥ 10 [18]	–

Fig. 8. Variation of microhardness over the thickness of ring specimens of alloy D16 after treatments *1*, *2*, *3*, *4* (Table 1): x) distance from the outer surface of the ring.

data of the x-ray diffraction analysis show that such treatment reduces the size of the blocks in rectangular specimens from 88 ± 11 to 70 ± 4 nm and the level of microstresses from 100 ± 12 to 56 ± 10 MPa.

The Vickers hardness in the surface zone of the specimens treated with the use of CTTS increases. The yield strength, the ultimate strength, the elongation and the contraction of alloy D16 have values matching the performance specification after natural and artificial aging. The negative effect of the reduction of the favorable compressive stresses in the surface zone of the articles is compensated by the hardening of the surface zone and by the lowering of the dangerous tensile stresses in the center of the articles. The lowering of the sizes and the growth of the density and of the uniformity of the distribution of particles of the hardening phase provided by the CTTS result in an increase in the ductility of alloy D16.

residual stresses are reduced from –230 to –190 MPa (by 17%) after natural aging and from –200 to –125% (by 38%) after artificial aging.

CONCLUSIONS

Heat treatment of alloy D16 including water cooling followed by cooling in liquid nitrogen to –196°C and subsequent oil heating to +175°C reduces the maximum residual macrostresses in the studied ring and rectangular specimens by 26% after natural aging and by 71% after artificial aging.

The use of cryogenic treatment and thermal shock (CTTS) changes the microstructure and the fine structure of the alloy. The plastic deformation due to the thermal shock at cryogenic temperature raises the dislocation density. When the alloy is aged, the density of the lath particles of the hardening phase increases and the density of the massive faceted particles decreases. The biaxial stress state in the surface zone of the articles gives rise to a strain texture. The CTTS reduces the thickness of the zone free of particles of the hardening phase due to their more uniform distribution. The

REFERENCES

1. T. Croucher, "Minimizing machining distortion in aluminum alloys through successful application of uphill quenching — A process review," in: L. Canale and M. Narazaki (eds.), *Quenching and Cooling, Residual Stresses and Distortion Control*, ASTM Int., West Conshohocken, PA (2010), pp. 332 – 351.
2. Yu. A. Puchkov, Y. Wang, A. Yu. Ampilogov, et al., "A study of the effect of quenching cooling rate on the structure and properties of alloy V91T3 of the Al – Zn – Mg – Cu system," *Tekhnol. Met.*, No. 8, 15 – 21 (2010).
3. Yu. A. Puchkov, Y. Wang, V. M. Polyanskii, et al., "A study of decomposition of supercooled solid solution of aluminum alloy V91 of the Al – Zn – Mg – Cu system," *Metalloved. Term. Obrab. Met.*, No. 8, 16 – 22 (2010).
4. I. Benarieb, Yu. A. Puchkov, G. G. Klochkov, et al., "A study of the effect of quenching cooling rate on the structure and properties of sheets from high-technology alloy V-1341 of the Al – Mg – Si system," *Materialovedenie*, No. 7, 43 – 48 (2019).
5. Yu. A. Puchkov, V. M. Polyanskii, and L. A. Sedova, "A study of the effect of modes of isothermal quenching on the structure and properties of aluminum alloy V-1341T," *Metalloved. Term. Obrab. Met.*, No. 2, 13 – 19 (2019).
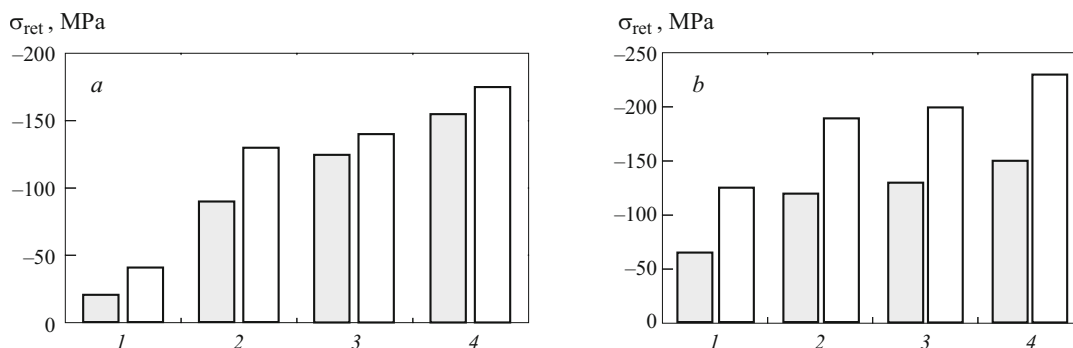
Fig. 9. Residual stresses in ring (*a*) and rectangular (*b*) specimens after treatments *1*, *2*, *3*, *4* (Table 1): the dark columns — minimum values; the light columns — maximum values.

6. I. Benarieb, Yu. A. Puchkov, G. G. Klochkov, et al., "Prediction of the effect of quenching mode on mechanical properties of sheets from heat hardenable aluminum alloy V-1341," in: *Role of Fundamental Researches in Implementation of "Strategic Directions of Advancement of Materials and Technologies of their Processing for up to 2030," Mater. IV All-Russia Conf.* [in Russian] (2018), pp. 58 – 70.

7. E. C. A. Simencio, G. E. Totten, and L. C. F. Canale, "Uphill quenching of aluminum: a process overview," *Int. Heat Treat. Surf. Eng.*, **5**(1), 26 – 30 (2011).

8. D. A. Lados, D. Apelian, and L. Wang, "Minimization of residual stress in heat-treated Al – Si – Mg cast alloys using uphill quenching: Mechanisms and effects on static and dynamic properties," *Mater. Sci. Eng. A*, **527**(13 – 14), 3159 – 3165 (2010).

9. Mai Huan Dung, Yu. A. Puchkov, and S. P. Shcherbakov, "A study of the effect of uphill quenching on residual stresses and properties of aluminum alloy D16," *Zagot. Proizvod. Mashinostr.*, **18**(3), 125 – 129 (2020).

10. Mai Huan Dung, Yu. A. Puchkov, A. I. Plokhikh, and I. Benarieb, "A study of the effect of heat treatment modes on quenching stresses and properties of steel D16," *Naukoemk. Tekhnol. Mashinostr.*, No. 4(106), 9 – 17 (2020).

11. Belinda Gruber, Imgard Weißenstreiner, Thomas Kremmer, et al., "Mechanism of low temperature deformation in aluminum alloys," *Mater. Sci. Eng. A*, **795**(23), 139935 (2020).

12. Mai Huan Dung, A. I. Gnevko, and Yu. A. Puchkov, "A study of the effect of cryogenic treatment on residual stresses and properties of aluminum alloy D16," *Aviats. Mater. Tekhnol.*, No. 2(59), 25 – 31 (2020).

13. Mai Huan Dung, A. I. Gnevko, et al., "Effect of cryogenic treatment and thermal shock on quenching stresses and properties of alloy D16," *Tekh. Tekhnol.*, No. 4(13), 473 – 486 (2020).

14. Mai Huan Dung, Y. A. Puchkov, and S. L. Berezina, "Influence of uphill quenching on residual stresses and properties of alloy D16," *Mater. Today, Proc.*, **38**(4), 1294 – 1298 (2021).

15. Hak-Jin Lim, Dae-HoonKo, Dae-CheolKo, and Byung-Min Kim, "Reduction of residual stress and improvement of dimensional accuracy by uphill quenching for al6061 tube," *Metall. Mater. Trans. B*, **45**(2), April, 472 – 481 (2014).

16. S. C. Wang and M. J. Starink, "Two types of S phase precipitates in Al – Cu – Mg alloys," *Acta Mater.*, **55**, 933 – 941 (2007).

17. J. R. Davis, *ASM Specialty Handbook. Aluminum and Aluminum Alloys*, ASM Int. (1993), 784 p.

18. *GOST 21488–97. Bars Pressed from Aluminum and Aluminum Alloys* [in Russian].